CHAPTER SEVEN

Thionitrous Acid/Thionitrite and Perthionitrite Intermediates in the "Crosstalk" of NO and H_2S

Juan P. Marcolongo, Ari Zeida, Leonardo D. Slep, José A. Olabe[1]
Facultad de Ciencias Exactas y Naturales and INQUIMAE, Universidad de Buenos Aires/CONICET, Ciudad Universitaria, Buenos Aires, Argentina
[1]Corresponding author: e-mail address: olabe@qi.fcen.uba.ar

Contents

Abstract

The chemistry of aqueous NO and H_2S as redox regulators of cellular and physiological responses in cardiovascular, immune or neurological tissues has raised the question of the overlapping pathophysiological functions often involving similar molecular targets. The interactions of NO with H_2S may functionally influence each other and focus has been directed to new N/S hybrid species eventually determining signaling capabilities. Besides the well-studied nitrosothiols, RSNOs, the eruption of H_2S in the mechanistic scene has stimulated increased interest in thionitrous acid, HSNO, and thionitrite, NOS^-, as well as in perthionitrite (nitrosopersulfide), S_2NO^-. We discuss the elusive chemistry of the latter molecules as intermediates in selected reactions in aqueous solution, either as

Advances in Inorganic Chemistry, Volume 70
ISSN 0898-8838
http://dx.doi.org/10.1016/bs.adioch.2017.02.002

free species or as bound to iron metal centers. The coordination chemistry involves mainly an updating on the "Gmelin" reaction proceeding upon mixing nitroprusside $[Fe(CN)_5(NO)]^{2-}$ and H_2S, with controversial and still unsolved mechanistic issues related to the onset of NO, HNO/N_2O, polysulfides HS_n^- ($n = 2–7$), together with bound thionitrous acid/thionitrite/perthionitrite and other intermediates and products.

1. INTRODUCTION

NO and H_2S, two molecules frequently named "gasotransmitters" *(1,2)*, accomplish diverse biological functions associated with animal *(3)* and plant *(4,5)* physiology: regulation of blood pressure, neurotransmission, immune response, as well as plant defense responses, stomata closure, abiotic stress, seed germination, etc. Both compounds are involved in aqueous 1-electron or multielectron redox chemistry with generation of species whose structure-reactivity behavior needs to be elucidated for discerning how the chemistry translates into a biological response. On the one hand, NO is a radical molecule able to react either as an oxidant or reductant *(2,6)*; it is ubiquitously placed in the redox system comprising the eight-electron interconversion between nitrates and ammonia, and affords a versatile mechanistic chemistry covered by the activity of several enzymes: NO—synthases, NO and NO_2^-—reductases, NH_3—oxidases, NH_2OH—oxidoreductases, etc. *(7)* On the other hand H_2S can only behave as a reductant; it may also produce up to 8-electron changes, with species in oxidation states in the range −2 to +6, i.e., from sulfides to sulfates *(8,9)*. The eventual availability and redox reactivity of O_2 may control the chemistry of each of the intermediates, which can also be influenced by the disposal of metal-binding coordination sites *(2,10)*.

The NO signaling cascade has been increasingly well characterized through the identification and chemical properties of distinct nitrosyl redox states NO^+, $NO^{\cdot}$, NO^-/HNO as intermediates in the oxidative or reductive cycles *(2,6)*. Less understood are the biological–pharmacological effects of sulfides; species other than H_2S might be responsible for signaling, like sulfane sulfur S^o, an uncharged species with six valence electrons having a unique ability to attach reversibly to other sulfur atoms as in elemental sulfur (S_8), persulfides (RSSH), polysulfides (HS_n^-, $n = 2–7$) thiosulfate $\left(S_2O_3^{2-}\right)$, and others *(11–13)*.

There is a growing appreciation that both H_2S and NO behave as messengers with connecting biochemistries *(14–20)*. In this NO/H_2S

"crosstalk" new biological mediators might be involved *(21)*, sustaining our focus on some early described N/S hybrid species, as advanced in Fig. 1. One of them is thionitrous acid, described generically as HSNO (other isomers have been described, see later) *(22)*, together with its conjugated base thionitrite SNO^- *(23)*, and perthionitrite S_2NO^- *(23)*, the sulfur analog of peroxynitrite O_2NO^-. H_2S plays a unique role in the generation and reactivity of the latter intermediates in a significantly different way as performed by thiols RSH, thus highlighting a hot topic in the emerging mechanistic bioinorganic chemistry relevant to the modification of proteins by H_2S *(24–27)*. In this context we deal with the chemistry of nitrosothiols, RSNOs *(28,29)*, with R = glutathione (GSH), cysteine (cysSH), etc., and we discuss the common and distinct chemical features compared to HSNO. We expand into the coordination chemistry aspects by updating on the mechanistic details of the reaction of nitroprusside $[Fe(CN)_5(NO)]^{2-}$ with H_2S, the "Gmelin" process, a fascinating sequence of reactions involving the onset of the three relevant iron intermediates: $[(NC)_5Fe(NOSH)]^{3-}$,

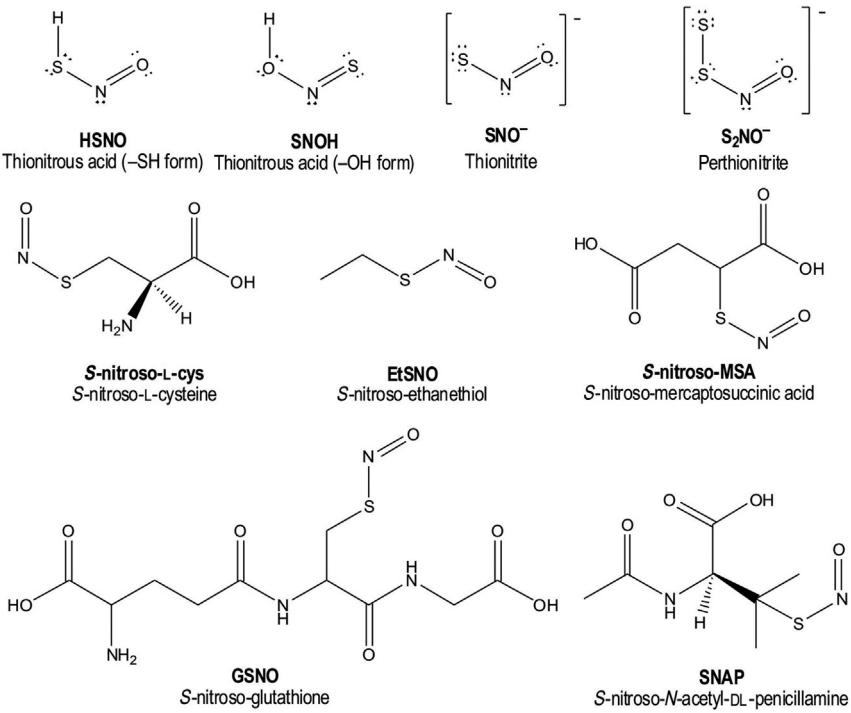

Fig. 1 Chemical structures of selected N/S hybrid species and *S*-nitrosothiols.

$[(NC)_5Fe(NOS)]^{4-}$, and $[(NC)_5Fe(NOS_2)]^{4-}$, all showing a complex mechanistic chemistry *(30–34)*.

2. *S*-NITROSOTHIOLS, RSNOs, A BRIEF OVERVIEW ON STRUCTURE AND REACTIVITY

S-nitrosothiols constitute a vast collection of compounds with properties dependent on the nature of the R group *(28,29)*. Fig. 1 includes a selected list with R = alkyl, aryl and other substituted species with relevance to biochemistry. RSNOs have been detected in vivo and are described playing a role of NO carriers, sinks, and reservoirs, with potential medical use as NO donors. Fig. 2 affords a structural description with two main resonance structures (I) and (II) *(29,35)*. The dominant contribution (I) comprises single and double S–N and N–O bonds, respectively. A greater contribution of (II) can be achieved by increasing the electron–donor abilities of R, influenced by the nature of substituents, or by N-binding to transition metals. Both factors contribute strengthening the S–N bond and weakening the N–O bond, with consequent effects on the reactivity. A third possible resonance "ionic" structure (III) $\{RS^-NO^+\}$ has not been included in Fig. 2 because of the minor relevance (it comprises a nitrosonium cation with a N–O bond order of 3).

RSNOs can be prepared by reactions of thiols with oxidizing NO derivatives such as NO_2, N_2O_3, nitrites, and organic nitroso compounds. In particular cases, NO can react with thiols yielding disulfides RSSR and N_2O *(28)*. RSNOs can be detected by using characteristic UV–vis, IR, and NMR signatures. UV–vis absorptions comprise three bands: an intense one at 225–261 nm ($\varepsilon \sim 10^4\ M^{-1}\ cm^{-1}$), a second one at 340 nm ($\varepsilon \sim 400$–$2000\ M^{-1}\ cm^{-1}$), and a weak one at 550–600 nm ($\varepsilon \sim 60\ M^{-1}\ cm^{-1}$). They have been assigned to allowed $\pi \rightarrow \pi^*$, $n_O \rightarrow \pi^*$, and forbidden $n_N \rightarrow \pi^*$ transitions, respectively (29). The IR spectra exhibit two characteristic peaks in the range of 1450–1530 and 610–685 cm^{-1}, both sensitive to ^{15}N substitution, attributed to ν_{NO} and ν_{NS} stretching, respectively. The nitroso group in RSNOs shows N–O distances in the range of 117–120 pm,

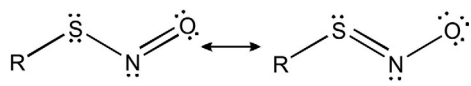

Fig. 2 Resonance structures of *S*-nitrosothiols.

shorter than in NO^- (126 pm) and longer than in NO^+ (106 pm) and $NO^\cdot$ (115 pm), supporting a bond order of ~2 *(28,29,35)*. Typical values for the N-S distances are at ~175 pm. The trends on the different properties of RSNOs can be discussed under the structural framework described in Figs. 1 and 2.

RSNOs undergo a variety of chemical reactions. A distinctive one is the spontaneous thermal decomposition giving NO and RSSR. It has been established that the half-life of different aqueous RSNOs varies from seconds to hours, or even days. Most importantly, decomposition rates are currently catalyzed by traces of metal ions, particularly by copper, a property that can be best controlled by using chelating agents such as dipicolinic acid (dipic) *(28,29,36)*. For these reasons, structural correlations are difficult to establish, a drawback that is reinforced by the influence of oxygen and light on the decompositions (irradiation of RSNOs at 340 and 550–600 nm produces $NO^\cdot$ and $RS^\cdot$ radicals) *(29)*. The uncatalyzed aqueous decomposition reaction has been proposed to be reversible, described by reaction (1):

$$RSNO \leftrightharpoons RS^\cdot + NO^\cdot \quad aq \tag{1}$$

The $RS^\cdot$ radicals may combine forming RSSR (Eq. 2), and can also react with thiolate RS^- to produce the very reactive $RSSR^{\cdot -}$ radical (Eq. 3), a source of $RSOO^\cdot$ in the presence of O_2. These radicals can be detected by spin-trapping techniques *(37)*.

$$2RS^\cdot \rightarrow RSSR \quad aq \tag{2}$$

$$RS^\cdot + RS^- \leftrightharpoons RSSR^{\cdot -} \quad aq \tag{3}$$

A high value of $\Delta G_1^\circ = +110$ kJ mol^{-1} has been estimated for reaction (1), for nitrosocysteine *(38)*. Therefore, we would hardly expect the uncatalyzed reaction (1) to proceed significantly to the right, unless a very fast removal of products were onset.

Reactions of RSNOs with RS^- are biochemically important. They comprise the 1,2-addition of RS^- at the N–O bond, followed by processes resulting in oxidation of sulfur and NO reduction. The nature of intermediates and products depends on the reagent ratios; thus, N_2O, NH_2OH, and NH_3 are produced under moderate excess of thiolate, whereas NH_3 is the only N-containing product at a higher excess. Different mechanisms have been proposed *(39–41)*. RSNOs can also be reduced by alcohols, amines, phosphines, etc. *(29)*.

A very important reaction of RSNOs inside a cell or in a biological fluid is the transnitrosation reaction (4):

$$RS^- + R'S'NO \leftrightharpoons RSNO + R'S'^- \quad aq \tag{4}$$

Reaction (4) comprises the reversible transfer of the *S*-nitroso functional group from a thiolate to another, and involves the nucleophilic attack of the thiolate anion on the nitroso nitrogen. It provides a route for the S-nitrosation or S-denitrosation of proteins. The equilibrium position of (3) depends on the forward- and reverse rate constants, whose values can vary in the range of 0.1–500 $M^{-1}\ s^{-1}$, according to the reactants. Transnitrosations can be enzyme-catalyzed (viz., with thioredoxins), and in general the kinetic/thermodynamics are important for describing the S-nitrosations that occur when exposing cells to low-molecular-mass RSNOs, a process for protein modifications without the involvement of NO. The factors influencing S-nitrosation of proteins may be different from those for other RSNOs *(28)*.

3. THIONITROUS ACID HSNO AND THIONITRITE SNO^-, ELUSIVE AQUEOUS INTERMEDIATES

Thionitrous acid, HSNO, is frequently referred to as the "smallest" and even the "simplest" nitrosothiol. The latter qualification seems questionable, given the availability of a mobile and ionizable H-atom in HSNO, thus allowing for inherent specific reactivity *(26,27,42)*. Back in 1952, four compounds were proposed to behave in a rapid equilibrium, Eq. (5) *(22)*:

$$HNSO \leftrightharpoons HOSN \leftrightharpoons HSNO \leftrightharpoons HONS \tag{5}$$

The four isomers have been characterized by IR spectroscopy in an argon matrix at −261°C (ν_{NO}, 1569 cm^{-1} for the HSNO *cis*-isomer), and were found to be light-sensitive and prone to polymerization. Looking for the biological relevance, the isomerization reactions have been computationally explored using high-level coupled-cluster as well as density functional theory (DFT) methodologies *(43)*. Gas-phase calculations show that the HONS tautomer and the Y-isomer SN(H)O are thermodynamically feasible, with energy differences close to the one for HSNO by ~25 kJ mol^{-1}. Notably, while the gas-phase isomerization barriers for HSNO into HONS and SN(H)O become prohibitively high, ~125–210 kJ mol^{-1}, the polar aqueous environment and water-assisted

proton shuttle decrease these barriers to ~37 kJ mol^{-1}, making the latter two isomers kinetically accessible under physiological conditions *(43)*.

Very recently, *cis*- and *trans*-conformers of HSNO have been prepared by mixing diluted H_2S and NO that react over metallic surfaces at room temperature *(44)*. Identification has been achieved by Fourier-transform microwave spectroscopy and quantum chemistry structural calculations, yielding significantly long S–N distances for the *cis*- and *trans*-species, 183.4 and 185.2 pm, respectively (cf. with ~175 pm for RSNOs). Although changes might be expected upon hydration, the results are quite significant for suggesting accessible homolytic/heterolytic paths for HSNO reactivity upon biorelevant conditions, as discussed below.

There are no reports on the pK_a of HSNO. A comparison with nitrous acid HONO (3.25) allows predicting that HSNO should be more acidic, thus converting to the anionic thionitrite form SNO^- in the biorelevant aqueous solutions at pHs ~7. A value of 2 has been very recently suggested *(45)*. By performing pulse radiolysis of anaerobic NO_2^-/H_2S mixtures, the difference spectra allowed proposing a value of 340 nm for the maximum in the UV–vis spectrum of HSNO, supported by a mass spectrometric (MS) identification of a protonated species *(24)*. This could be considered a tentative value, casting some doubt on the putative coexistence of SNO^-, given that the pH used was as high as 11. Recent modern computational work led to calculated weak absorptions at 315 and 360 nm for HSNO in water (Table 1) *(49)*. A value at 315 nm was calculated for SNO^- in acetonitrile, fairly close to the experimental value in the same solvent, 323 nm *(23)*.

Care should be exercised when discussing the meaning of macroscopic acidity constants of systems which can be protonated in nonequivalent sites. Although each one of the conjugated weak acids has a microscopic acidity constant (K_{ai}), the system behaves macroscopically as if only one weak acid in equilibrium with its conjugated weak base existed in solution. This is so simply because the different K_{ai} constants freeze the ratio between any pair of protonated species (and eventually also for any two unprotonated ones) making these values pH-independent. In such a system the apparent equilibrium constant K_{ap} is given by $K_{ap}^{-1} = \sum_{i=1}^{n} K_{ai}^{-1}$. In the specific situation where the dispersion of the individual K_{ai} is high, the value of K_{ap} is dominated by the acid/base with the weakest microscopic K_{ai} *(50)*. In the present case this would be NSOH, for which an estimation of p$K_a \sim 10$–11 appears as reasonable.

Table 1 TD-DFT Electronic Spectral Calculations of N/S Hybrid and Related Species in Water, Methanol, and Aprotic Solvents

Compound	Solvent	λ_{max} Exp (nm)	λ_{max} Calcd (nm) (Osc. Str., a.u.)
$[S_2NO]^-$	H_2O	409 *(46)*–412 *(26,27)*	411 (0.03)[a]
	Methanol	425 *(23)*	431 (0.025)[a]
	Acetone	448[b] *(24,25)*	458 (0.03)[a]
	Acetonitrile	450 *(25)*	458 (0.02)[a]
$[O_2NO]^-$	H_2O	302 *(47)*	307 (0.03)
	CH_2Cl_2	340 *(47)*	339 (0.04)
EtSNO	H_2O	330[c] *(48)*	280, 310, 330[d]
ON(SH)S	Acetonitrile	358[e] *(25)*	368 (0.05)
HON(S)S	Acetonitrile	358[e] *(25)*	351 (0.4)
HSNO	Water	340[f] *(24)*	315, 360[d]
SNO^-	Acetonitrile	323 *(23)*	315 (0.02)

[a]Reported in Ref. *(49)*, with the exception of the value for methanol.
[b]Also measured at 448 nm in DMSO or DMF in Ref. *(46)*.
[c]Observed as a shoulder in the spectra of aqueous $[Fe^{II}(CN)_5(NOSR)]^{3-}$ ions. Also measured at 330–350 nm with free thiols in organic solvents *(29)*.
[d]Low intensity absorption bands.
[e]Assigned as a mixture of isomers ON(SH)S and HON(S)S.
[f]Generated by pulse radiolysis of deoxygenated solutions, pH 11.
For the oscillator strengths, a damping factor $\gamma = 0.2$ fs^{-1} was used.

Low concentrations of sulfide were shown to quench NO-mediated vascular responses through formation of an uncharged nitrosothiol, assumed to be HSNO *(14)*. An attempt to prepare and characterize HSNO in aqueous solution at pH 7.4 has been reported by Filipovic and coworkers *(24)* by studying the transnitrosation of nitrosoglutathione GSNO with H_2S, reaction (6).

$$GSNO + HS^- + H^+ \rightarrow HSNO + GSH \tag{6}$$

The uncharged character of HSNO favors its ability for crossing membranes and provides a new scenario for the modulation of the RSNO profile in cells through the transnitrosation with cysteine residues in proteins, reaction (7).

$$HSNO + P - SH \leftrightharpoons PSNO + HS^- + H^+ \tag{7}$$

For reaction (6), the mixture of reactants at pH 7.4 induced the decay of the UV–vis main band of GSNO (λ_{max}, 334 nm) with onset of a moderately stable intermediate, I_{yellow}, with λ_{max} at 412 nm *(24)*. Fig. 3 shows a similar picture evolving at pH 10 *(51)*. Related reactions were also studied with *S*-nitrosocysteine (CysNO), *S*-nitrosopenicillamine (SPEN), and *S*-nitroso-*N*-acetylpenicillamine (SNAP) *(26,51)*.

For GSNO, the UV–vis display (pH 7.4 or 10) did not match with the stoichiometry of reaction (6), given that HSNO has been reported to absorb at 330–340 nm, not at 412 nm *(24,49)*. The band of HSNO might be hidden below the absorption of GSNO or it could rapidly decay in terms of the reactivity of HSNO at room temperature. The MS positive evidence for HSNO obtained with cryogenic experiments *(24)* has been complemented by some UV–vis evidence appearing in the reaction of HS^- with SNAP through the onset of a transient species with λ_{max} at 320 nm, assigned to SNO^- *(26)*. Transnitrosation reactions such as in Eqs. (4) and (6) are reversible processes, though under pH 7.4 conditions, the poor nucleophilicity of GSH could hardly ascribe a significant rate to the reverse reaction. By measuring the decrease of $[HS^-]$, a value of $k_6 = 84\ M^{-1}\ s^{-1}$ has been reported *(24)*.

The aqueous reactivity of HSNO has been under close scrutiny given its potential ability to form a second generation of intermediates with putative specific signaling roles *(24–27)*. Closely related to reaction (1), reaction (8a) implies the homolytic cleavage of the S–N bond with the production of NO

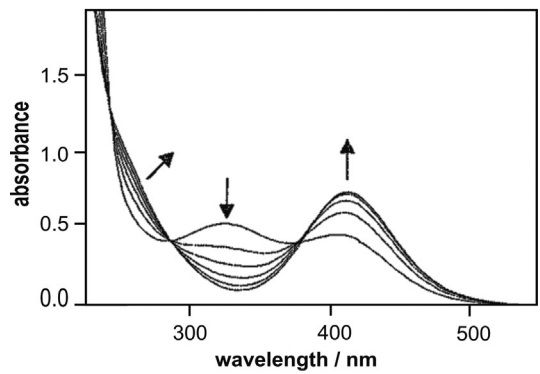

Fig. 3 Transnitrosation reaction of 10^{-3} M GSNO and HS^-, pH 10. Decay of GSNO at 334 nm and build-up of I_{yellow} at 412 nm. *Adapted from Munro, A. P.; Williams, D. L. H.* J. Chem. Soc. Perkin ***2000***, 21, *1794–1797, with permission of The Royal Society of Chemistry.*

and reactive $S^{\bullet -}$ radicals (8b). Under the availability of HS^-, the formation and reactivity of $HS_2^{\bullet 2-}$ radicals (8c) may produce NO and disulfides irreversibly under catalytic conditions (8d), given the strong reducing power of $HS_2^{\bullet 2-}$: *(52)*

$$HSNO \leftrightharpoons NO^{\bullet} + HS^{\bullet} \quad (aq) \tag{8a}$$

$$HS^{\bullet} \leftrightharpoons S^{\bullet -} + H^+ \quad (aq) \quad pK_{8b} = 3.4 \ (\text{Ref. } 52) \tag{8b}$$

$$S^{\bullet -} + HS^- \leftrightharpoons HS_2^{\bullet 2-} \quad (aq) \quad K_{8c} = 9 \pm 2 \times 10^3 M^{-1} \ (\text{Ref. } 52). \tag{8c}$$

$$HS_2^{\bullet 2-} + HSNO \rightarrow NO^{\bullet} + HS_2^- + HS^- \quad (aq) \tag{8d}$$

Related to the influence of the bond dissociation energies (BDE) in the rates of homolysis reactions *(28,29)*, the comparatively long N–S bond in HSNO is weaker than in RSNOs by ~12 kJ mol^{-1} *(38)*, consistent with the relative electron-withdrawing abilities of H and R. The BDE for *cis*-HSNO has been calculated to be 123–127 kJ mol^{-1} *(43,44)*.

A second reactivity mode for HSNO has been proposed through reaction (9), similarly as demonstrated for thiolates RS^- acting as nucleophiles toward the S-atom in RSNOs *(41)*. Hydrodisulfides are also direct products, along with HNO. This reaction has also been proposed to occur in the metal-catalyzed reactions of NO and H_2S in the presence of excess of the latter reagent *(44)*.

$$HSNO + HS^- \leftrightharpoons HNO + HS_2^- \tag{9}$$

Although reaction (9) has been described as endergonic ($\Delta G_9^{\circ} = +32$ kJ mol^{-1}) *(45)*, it might be plausible under conditions of fast products removal. HNO (a precursor either for the fast generation of N_2O or for subsequent reduction) has been detected after mixing GSNO and H_2S; this is a remarkable fact *(24)*, though other routes for HNO generation could onset, namely the direct reaction of NO with HS^- *(53)*, or the ensuing decomposition of perthionitrite *(25)*. A high reactivity for HS_2^- can also be anticipated, as seen later.

It should be noted at this point that neither of the above analyzed reactions account for the absorption properties of I_{yellow}, the moderately stable intermediate with λ_{max} at 412 nm formed after mixing the GSNO/HS^- reactants in the transnitrosation reaction (6), as can be seen in Fig. 3. The analysis requires describing the fast reactivity of hydrodisulfides; one of these reactions leads to polysulfides, as discussed later.

4. POLYSULFIDES AND SULFUR SOLS

Currently polysulfides can be produced through the partial oxidation of sulfides. They have been reported to be formed after the onset of the transnitrosation reactions such as in Eq. (6) through the subsequent disproportionation reactivity of the HS_2^- intermediate *(24)*. The build-up of polysulfides can proceed sequentially under available oxidizing conditions by adding a varying number of sulfur atoms to HS^- yielding soluble sulfane chains, as described in reaction (10). The fast processes for HS_n^- generation can be followed by a slower one comprising separation as colloidal sulfur, ending in S_8 *(36,54)*.

$$HS^- \leftrightharpoons HS_2^- \leftrightharpoons HS_3^- \leftrightharpoons \ldots \leftrightharpoons HS_9^- \rightarrow S_8 + HS^- \qquad (10)$$

Polysulfide formation currently arises *after* the exhaustive consumption of the oxidizing substrate in reactions such as shown in Eq. (6), also observed upon mixing peroxynitrite with HS^- *(55)*. Polysulfides are relatively stable at pHs ≥ 7, but disproportionate under more acidic conditions, reaction (11).

$$HS_{(n+1)}^- \rightarrow n/8S_8 + HS^- \quad (n = 1-8) \qquad (11)$$

Colloidal sols (sulfur/polysulfide mixtures) may be formed at pHs ≤ 8, usually in the second-time scale, depending on the medium, relative reactant concentrations, and/or variable mixing modes that might determine a high local concentration of a given reactant. By assuming a fast reactivity of disulfides, the colloidal sols have been proposed as responsible for the onset of the 412 nm band assigned to I_{yellow} *(24,25)*. The physical and chemical properties of aqueous polysulfides are not clearly understood; their most intense electronic absorptions are reported to occur at wavelengths $\leq$300 nm *(56)*; much weaker bands have been reported for commercial samples with maximum wavelengths <400 nm for different HS_n^- species ($n = 2$–5). Our calculations with the quantum mechanics-molecular mechanics (QM) – (MM)/(DFT) methodologies are in agreement with the latter observations.

Even though some disproportionation of HS_2^- is expected at pH 7.4, the "in situ generation" of HS_2^- in a colloidal environment still allows a favorable competitive reactivity with other substrates *(42)*, as will be analyzed below seeking for a convincing explanation on the properties of I_{yellow}.

5. PERTHIONITRITE, S_2NO^-. IDENTIFICATION OF I_{YELLOW}

5.1 Available Results

Munro and Williams already suggested in 2000 that I_{yellow} could be identified as S_2NO^- *(51)*, supported by the X-ray structure obtained by Seel, Krebs, and coworkers in 1985 of the [PNP][S_2NO] salt (PNP^+ =Bis(triphenyl)phosphaniminium), isolated from an acetone solution after mixing [PNP][NO_2] with elementary sulfur or a PNP-polysulfide, under anaerobic conditions *(23)*. Although the solid was soluble only in aprotic solvents with λ_{max} at ~450 nm, absorption transients at 409 nm appeared upon mixing NaHS/Na_2S_2 with NO in aqueous solutions *(46)*. Moreover, intermediate values at 425 nm were measured in methanol or ethanol *(46)*. The picture suggests a solvatochromic behavior for the perthionitrite anion, as recently demonstrated by QM-MM molecular dynamics (MD) simulations combined with a real-time TD-DFT analysis *(49)*, which we discuss later.

Filipovic and coworkers claimed providing negative spectroscopic evidence (IR, ^{15}N NMR, MS) for S_2NO^- eventually arising subsequently to the onset of reaction (6) *(24)*. In fact, they reported a shift in the IR-stretching frequency up to 1 min after mixing (1515 → 1568 cm^{-1}), presumably due to changes in ν_{NO} for the GSNO → HSNO conversion; we believe that the shift could be traced alternatively to GSNO → S_2NO^-, assuming that perthionitrite is the actually observed species in the UV–vis experiment on such a minute time scale *(24)*. On the same grounds, the ^{15}N NMR signal at 322 ppm in water, traced to HSNO *(24)*, could alternatively correspond to S_2NO^-, consistent with the recently reported value at 332 ppm, traced to its NBu_4^+ salt in tetrahydrofuran (THF) *(57)*. Further ambiguity arises if we consider that rapidly interconverting HSNO/S_2NO^- mixtures could exist in the solution (see later) giving a ^{15}N NMR signal corresponding to an averaged feature. In a crucial experiment, Feelisch and coworkers obtained positive electrospray ionization (ESI)-high-resolution mass spectrometry (HRMS) signals derived from aqueous SNAP/HS^- mixtures at pH 7.4, consistently assigned to S_2NO^- *(27)*. A very recent report states that S_2NO^-, generated by mixing Na_2S and GSNO at a 2:1 ratio in buffered solution at pH 7.4, can be handled in anaerobic medium in a controlled manner, showing a slow decay of the band at 412 nm, with 80% absorbance remaining in 3 h. The decay rate was enhanced in the presence of dioxygen *(58)*. Finally, Grman, Jacob, and coworkers *(20)* showed very recently that the reaction of GSNO with

organic polysulfanes $R-S_x-R'$ ($x = 1-4$), at pH 7.4 and in the presence of cysSH or GSH, led to the build-up of I_{yellow} at 412 nm, identified as S_2NO^-. Its formation and decomposition occurred in 15–40 min under the studied conditions, with release of NO. Mixtures of GSNO/polysulfanes in the absence of cysSH or GSH were not reactive, i.e., the addition of either of the latter reagents was required in order to generate HS^-, suggesting that the reaction evolves similarly as in the transnitrosation process initiated by reaction (6).

A claim was also raised on the intrinsic instability of S_2NO^- in water toward the rapid formation of HNO and sulfur, either in acidic or neutral conditions *(25)*. By using a freshly prepared solution of [PNP][S_2NO] in acetone, followed by dissolution either in a 10%–water/acetonitrile mixture or in a sulfide-containing aqueous solution at pH 7.4, the authors reported the formation of a species with λ_{max} at ~420 nm in a few seconds, which survived for minutes along with a slow decay, yielding an intermediate at ~340 nm reported as HSNO. The 420-nm peak emerged over the broad tail of a very intense UV-band centered at ~300 nm in a highly scattering medium, with the consequent assignment of the 420 nm absorption to a colloidal sulfur sol. In fact, we believe that the relevant S_2NO^- species has been missed through a wrong interpretation, as suggested later by our computational work on the UV–vis spectra *(49)*.

5.2 Absorption Spectra Calculations

The absorption spectra for S_2NO^- and related species were calculated by averaging an ensemble of instantaneous configurations sampled through QM-MM MD simulations. Spectral line shapes were obtained by complementary real-time TD-DFT calculations, a methodology that has proved reliable to predict the absorption properties of molecules and ions in solutions and complex environments *(49)*. Fig. 4 reinforces the assignment of the species absorbing at 409–412 nm in water to S_2NO^-. Most importantly, the experimentally observed bathochromic shifts when proceeding from water to other less-protic solvents is faithfully reproduced by the computational analysis. The main character of the UV–vis electronic transition is $p(S) \rightarrow \pi^*(SNO)$. Our calculations show that the absorption maximum for this molecule is strongly dependent on the geometrical parameters explored across the MD. Thus, the specific interactions with the solvent become extremely important to describe the spectroscopic behavior in solution.

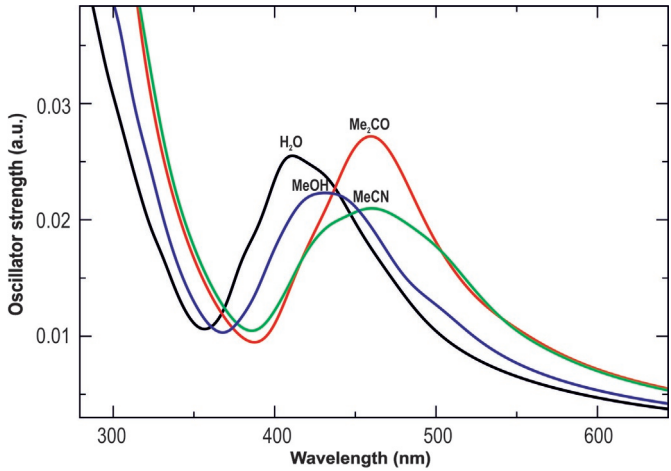

Fig. 4 Calculated electronic spectra for S_2NO^- in water (*black*), methanol (*blue*), acetone (*red*), and acetonitrile (*green*), using TD-DFT and QM-MM molecular dynamics simulations.

We have placed the computational methodology under a control system by performing calculations with other well characterized similar species, as detailed in Table 1, and excellent agreement with experimentally obtained UV–vis spectra have been found.

Most remarkably, it can be seen that the results with O_2NO^- also account for the experimentally observed solvatochromism *(47)*. Solvatochromic effects have been observed for coordination compounds interacting with acceptor solvents. The big UV–vis and IR spectral shifts could not be accounted for by a mere dielectric effect as produced by a continuum solvent model, and empirical donor–acceptor correlations were employed with some success *(59)*. Consistently, a recently reported lack of correlation emerged by plotting the values of λ_{max} for S_2NO^- in different solvents against the corresponding dielectric constants *(60)*. However, in that report the authors highlighted that water did not fit in a linear correlation displayed by the alcohols, and interpreted that deviation as evidence for rejecting the 412 nm maximum as characteristic of S_2NO^- *(24,25,60)*. For all the used solvents, our results (Fig. 4, including alcohols) show that the specific interactions arise both from solvent-induced structural changes and from electrostatic solute–solvent effects, the former being dominant. It becomes clear that the strong H-bonding interactions in water differ from those arising in alcohols.

In a very recent work dealing with the NO/H_2S crosstalk, Pluth and coworkers reported on the reactions of diverse isolated persulfides RSSH

with NO_2^- in THF to produce NO via polysulfide and perthionitrite intermediates *(57)*. S_2NO^- was identified through a strong band at 446 nm, a feature also generated by independently mixing NO_2^- with S_8. To the coincidence of λ_{max} in THF with the values displayed in Table 1 for the aprotic solvents must be added the shift toward ~420 nm when using mixtures of 1:1 THF/H_2O. The ^{15}N NMR signal at 332 ppm in THF, assigned to $S_2{}^{15}NO^-$, appears to be related to the significant solvent structural influence, and suggests the best assignment of the aqueous 322 ppm signal to $S_2{}^{15}NO^-$ rather than to $HS^{15}NO$, as analyzed earlier *(24)*.

5.3 Consistency With X-ray Structural Data

Table 2 shows a comparative picture of new X-ray diffraction results *(25)* (which are essentially the same as originally reported) *(23)*, with data for the calculated species in solution *(49)*, presently expanded by including methanol as solvent.

A fair agreement with the reported *cis*-structure for the anion can be observed, with a trend to greater distance values in the calculated solution spectra that can reasonably be traced to packing and environmental effects.

Table 2 Selected Distances and Angles With Standard Deviation for Solid [PNP][S_2NO] (PNP^+ = Bis(Triphenyl)Phosphaniminium) *(25)*, and for the Anionic Species in Water, Methanol, Acetone, and Acetonitrile, Calculated Through Molecular Dynamics (MD)[a]

Parameter	DRX *(25)*	MD (H_2O)	MD (MeOH)	MD (Me_2CO)	MD (MeCN)
$d(N_1\text{-}O_1)$ (Å)	1.25 (0.01)	1.24 (0.03)	1.24 (0.02)	1.24 (0.02)	1.24 (0.04)
$d(N_1\text{-}S_1)$ (Å)	1.70 (0.01)	1.79 (0.01)	1.78 (0.06)	1.80 (0.07)	1.80 (0.08)
$d(S_1\text{-}S_2)$ (Å)	1.97 (0.01)	2.07 (0.06)	2.04 (0.04)	2.03 (0.04)	2.04 (0.04)
$\theta(O_1\text{-}N_1\text{-}S_1)$ (degree)	117.8 (0.2)	119 (5)	119 (4)	120 (4)	120 (4)
$\theta(N_1\text{-}S_1\text{-}S_2)$ (degree)	115.1 (0.2)	111 (5)	113 (5)	117 (6)	117 (5)

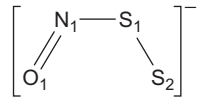

[a]Reported in Ref. *(49)*, with the exception of the value for methanol.

No significant changes can be observed by comparing the geometrical features of $S_2{}^{15}NO^-$ in the aprotic solvents, though subtle trends appear with data for methanol and water. The onset of hydrogen bonds between the negatively charged terminal sulfur S_2 ($q(S_2) \sim -0.7$) and NO ($q(NO) \sim -0.3$) fragments with the solvent determine a much lower (N_1-S_1-S_2) angle in water with respect to acetone and acetonitrile, with an intermediate value pertaining for methanol. This accounts for the observed spectral band shift to higher energies observed in water. Interestingly, this description is also in agreement with the reported small bathochromic shift when changing to alkaline solutions *(27)*, implying a weaker H-bonding array.

5.4 Chemical Routes Following Transnitrosation of RSNO With H_2S

A third possible route for the decay of HSNO has been proposed, reaction (12) *(49)*, on the basis of the early generation of hydrodisulfides in the medium. It is similar to a transnitrosation reaction, specifically a transnitrosopersulfidation one *(5)*.

$$HSNO + HS_2{}^- \rightleftharpoons S_2NO^- + HS^- + H^+ \tag{12}$$

The interchange between the nucleophiles hydrodisulfide and hydrosulfide at the NO group can be described as a S^o (sulfane)-atom transfer. It appears as a kinetically favored reactivity mode of HSNO, compared to reaction (9). We expect a greater value for the specific rate constant k_{12} than for k_9, on the basis of a greater nucleophilic ability of the more polarizable $HS_2{}^-$ over HS^- (see later for comparative measurements with the bound species). This is in agreement with predicted and observed trends for persulfides and thiolates *(61)*. Additional routes to S_2NO^- generation can be imagined, however, namely the attack of $HS_2{}^-$ on the still unconverted GSNO, and the reaction of NO with the putatively formed perthiyl radical, $S_2{}^{\bullet -}$, reactions (13)–(15).

$$GSNO + HS_2{}^- \rightleftharpoons S_2NO^- + GSH \tag{13}$$

$$S^{\bullet -} + HS_2{}^- \rightleftharpoons HS^- + S_2{}^{\bullet -} \tag{14}$$

$$S_2{}^{\bullet -} + NO^{\bullet} \rightleftharpoons S_2NO^- \tag{15}$$

Reaction (13) implies the attack of $HS_2{}^-$ toward the initial, still unconsumed GSNO reactant. Although HSNO can be predicted to be more electrophilic than GSNO, the effective variable concentrations of GSNO and HSNO might lead to reactions (12) and (13) proceeding with similar rates.

On the other hand, although reaction (14) has not been reported, it could proceed faster than (8c), given the expected favorable nucleophilicity of HS_2^- over HS^- toward the $S^{\bullet -}$ radical. In fact, a thermochemical estimation allows obtaining $\Delta G^o_{14} = -62$ kJ mol^{-1} *(45)*. Perthiyl radicals $S_2^{\bullet -}$ have been characterized and described as more stable species than $S^{\bullet -}$ *(62)*. They have been proposed to participate both in the generation and in the homolytic decomposition of S_2NO^- during the H_2S-transnitrosation processes, through reaction (15) *(27)*.

The above presented complex picture has been tested through simulation procedures, and the details on the assumed reactions and constants are analyzed as follows. Fig. 5 shows the traces for the decay of the initial reactants and the build-up of different intermediates in a restricted time window, for 0.5 mM GSNO and H_2S, mimicking the conditions used in Ref. *(24)*. We considered reaction (6) as irreversible, given the negligible nucleophilic reactivity of GSH, with $k_6 = 84$ M^{-1} s^{-1} *(24)*. For the equilibrium reaction (8a), we used $k_{8a} = 0.12$ s^{-1} (as measured by the [NO] build-up) *(24)*, and $k_{-8a} \sim 10^7$ M^{-1} s^{-1} (an estimated value for a rapid radical recombination). The required data for reactions (8b) and (8c) were taken from Ref. *(52)*. The value of $K_9 \sim 0.05$ was estimated by assuming values for $k_9 = 500$ M^{-1} s^{-1} and $k_{-9} = 10^4$ M^{-1} s^{-1}. K_9 was considered lower than K_{12} ($K_{12} \sim 100$–1000, with $k_{12} = 10^5$ M^{-1} s^{-1} and $k_{-12} = 10^3$ M^{-1} s^{-1} at pH 7) *(49)*, consistently with the smaller reactivity of thiolates in comparison with persulfides *(60)*. The consumption of HNO was traced either to reaction (16) yielding N_2O *(63)* or to reaction (17) giving HSNHOH *(64)* with further timely production of NH_2OH. Rate constants for the reactions of

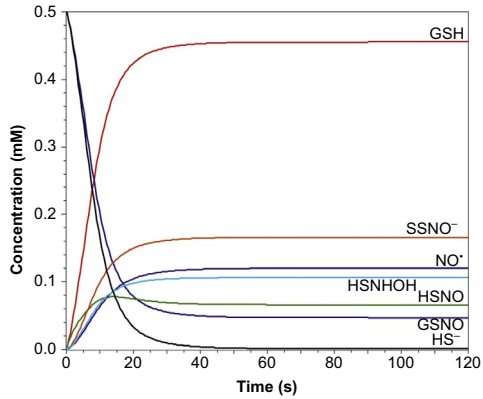

Fig. 5 Simulated traces for selected species when mixing 0.5 mM GSNO and H_2S, as described in the text.

HS_2^- with different substrates were estimated as being 100/1000-fold greater than for corresponding reactions with HS^-.

$$2HNO \rightarrow N_2O + H_2O \quad k_{16} = 8 \times 10^6 M^{-1} s^{-1} \text{ (Ref. 63)}. \tag{16}$$

$$HS^- + HNO \rightarrow HS - NHOH \quad k_{17} = 1.2 \times 10^6 M^{-1} s^{-1} \text{ (Ref. 64)}. \tag{17}$$

The simulation results for the concentration profiles show a consistent decay of [GSNO] (down to 90%), a consistent similar increase of [GSH], and a 100% decay of [HS^-]. The latter feature indicates that the initial trans-nitrosation step has not been completed under the proposed regime of reactions and that HS^- displays additional reactivity with the intermediates in order to attain a full consumption. The build-up of S_2NO^-, NO, and HSNHOH is onset after a short induction period and attains saturation in ~30 s, while [HSNO] grows exponentially up to a maximum for ~15 s and then decays slowly. The duration of the induction period (a few seconds) is reasonably accounted for in the allowed time window, if compared with the value estimated by us from the reported absorbance traces *(24)*. The attained concentration of S_2NO^- in the simulations is consistent with the available experimental data *(24)*, revealing a yield of ~30% (based on the reported value of $\varepsilon = 3125\ M^{-1}\ cm^{-1}$ in acetone *(25)*, which we presume similar to the one in water). It becomes evident that the formation of S_2NO^- competes with the generation of other nitrogenated products derived from the HSNO reactivity; importantly, the sum of N-containing products (S_2NO^-, HSNO, NO, HSNHOH) in the proposed time window of Fig. 5 is well close to 100% with respect to initial GSNO. On the other hand, [HNO], [HS_2^-] could not be established, suggesting a negligible concentration in the steady state. Neither N_2O was found in the simulations, presumably because dimerization of HNO is less favorable that its reactivity toward further reduction by HS^- (in fact, N_2O was not detected experimentally under the used equimolar concentrations of reactants, it was only observed for increasing sulfide concentrations) *(24)*. Indeed, variations in the simulations output could be obtained by further manipulation of the unreported rate and equilibrium constants, or considering alternative routes for NO/HNO decay (such as the possible intermediacy of hyponitrite radicals, $HN_2O_2^{\bullet -}$, as precursors of competitive N_2O/NH_2OH generation) *(65)*. Noticeable is the previously unreported induction period *(24)*, which is in contrast with the observations reported for the reactions of peroxynitrite *(55)* and SNAP *(26)* with HS^-.

The onset of reaction (12) makes the GSNO consumption through reaction (6) autocatalytic with respect to HS_2^-. It also provides an explanation for the net $GSNO \rightarrow S_2NO^-$ conversion (334 nm → 412 nm) and the absence of specific UV–vis spectral features for HSNO *(24)*. Autocatalysis is frequently associated with the build-up of induction periods for the generation of product, showing S-shaped traces *(66)*. In the underlying conditions, a requirement of sulfur radicals (reactions 8a–8d) seems crucial for the generation of the more reactive HS_2^-. The induction times have been reported to increase with $[O_2]$ and to decrease with $[HS^-]$ *(29)*, and this fact relates to the observed early consumption of O_2 *(26)*, a trapping agent for $S^{\cdot -}$ and $HS_2^{\cdot 2-}$ *(37)*. Overall, these autocatalytic features constitute favorable and specific evidence supporting the proposed mechanism highlighting the role of disulfides in biochemistry.

As a conclusion on the validity of the simulation procedures, we should remark that only a limited set of experimental conditions has been considered, namely the equimolar $GSNO/HS^-$ situation *(24,51)*. Indeed, a wider experimental approach is needed for testing the influence of increased $[HS^-]/[RSNO]$, changing the type of used RSNOs, as well as better disclosing the stoichiometric results under exhaustive conditions (viz., the yields of N_2O, NH_2OH, or eventually NH_3 and the conditions for the onset of polysulfides) *(24)*.

6. COORDINATION CHEMISTRY OF NITROSOTHIOLS, THIONITROUS ACID, THIONITRITE, AND PERTHIONITRITE

6.1 Nitrosothiols

RSNOs are potential ligands with at least three donor atoms, N, S, and O. Only N- and S-bonded coordination modes have been characterized. Substituted *S*-nitrosothiols may contain other coordination sites as –OH, $–NH_2$, –COOH, and others *(29)*.

Coordination to metal centers may change considerably the stability of RSNOs, depending on the nature of the metal and the ligand structure. The electron-rich metal ions Hg(II), Cu(II), Cu(I), Ag(I) prefer binding by the S-donor atom, thus destabilizing RSNOs. On the other hand, Fe(II) complexes usually lead to N-bonded RSNOs; they can be formed by ligand exchange, and usually lead to more stable complexes toward N–S bond rupture than the free RSNOs. We exemplify this with two

biorelevant cases, iron(II) dinitrosyls (DNIC) and cyano(L)ferrates(II), reactions (18) and (19) *(29)*:

$$Fe^{II}L_2aq + 2RSNO \rightarrow Fe(L_2)(NOSR)_2 \rightarrow Fe^{II}L_2(NO)_2 + RS^{\cdot} + RS^{-} \ (L = \text{cysteine, histidine, etc.}) \quad (18)$$

$$\left[Fe^{II}(CN)_5(L)\right]^{3-} + RSNO \leftrightharpoons \left[Fe(CN)_5(NOSR)\right]^{3-} + L(L = H_2O,\ NH_3,\ \text{etc.}) \quad (19)$$

For the cyano complexes, the iron-bound species have a variable stability, depending on R, and may decompose through dissociation (reverse of reaction 19) or through redox processes (homolysis at the N–S bond) as described by reaction (20) *(67)*.

$$\left[Fe(CN)_5(NOSR)\right]^{3-} \leftrightharpoons \left[Fe(CN)_5(NO^{\cdot})\right]^{3-} + RS^{\cdot} \quad (20)$$

The lifetimes and yields of the decomposition products are very variable, depending on the thiol structure, namely the inductive effects of the functional groups in R. Thus the complex with cysteine has a $t_{½}$ of 140 s, which can be increased by acetylation of the NH_2 substituent ($t_{½}$, 450 s), whereas it is shortened by esterification of the COOH group ($t_{½}$, 70 s). The mercaptosuccinic acid complex is remarkably stable ($t_{½} > 3.6$ h) *(29)*.

The UV–vis spectra of the $[Fe^{II}(CN)_5(NOSR)]^{3-}$ complexes are almost independent of the nature of the thiol, with two bands at ~525 and ~320 nm, with the former three to five times stronger *(67–69)*. These complexes have been also characterized by IR spectroscopy, with typical ν_{NO} stretching modes at 1380 cm^{-1} (NOSEt) *(69)* or 1390 cm^{-1} (NO-mercaptosuccinate) *(70)*. These values are significantly smaller that those observed with free nitrosothiols (viz., 1505 cm^{-1} for mercaptosuccinic acid) *(67)*, reflecting the σ–π bonding interactions with the metal. For the mercaptosuccinic complex, a value of 758 cm^{-1} has been reported for ν_{NS}, reflecting a much stronger N–S bond than in the free thiol ($\nu_{NS} < 700$ cm^{-1}) and consistent with the greater thermal stability in the bound situation *(70)*. NMR characterizations have been also published, with δ at 607 ppm (for ^{15}N) and at 1035 ppm (for ^{17}O) *(33,70)*.

Other metal centers (Ru, Rh, Ir, Os) with octaethyl- and tetraphenylporphyrin coligands have been used to model the interactions of RSNOs in biologically relevant iron–heme complexes *(29)*. A valuable mechanistic study has been provided for the reaction of RSNO: *N*-acetyl-1-amino-2-methylpropyl-2-thionitrite, with a model metalloporphyrin, Ru^{II}(OEP)(CO) (OEP = octaethylporphyrinato dianion) in

dry toluene or benzene *(71)*. The addition product *trans*-Ru^{II}(OEP)(NO)SR has been fully characterized by X-ray and spectroscopic methods and is stable only as a solid, decomposing under air, moisture, and light. The mechanism involves the initial rapid equilibrium formation of an S-bound Ru^{II}(OEP)(RSNO)(CO) intermediate, which leads to a short-lived second species in a rate-limiting step, Ru^{III}(OEP)(SR)(CO), presumably through S–NO bond cleavage.

An unusually stable iridium complex was obtained through the reaction of K[$IrCl_5$(NO)] with $PhCH_2SH$ in acetonitrile solution. The *trans*-K[Ir(CH_3CN)N(O)SCH_2Ph] salt was obtained by recrystallization from CH_3CN, and an X-ray structure could be solved *(72)*. The complex was characterized by UV–vis and ^1H NMR in CH_3CN and by FTIR spectra in the solid state, with ν_{NO} at 1443 cm^{-1} and ν_{NS} at 778 cm^{-1}, both sensitive to ^{15}N labeling. Note the upshift of ν_{NO} compared to the Fe(II) complexes described earlier, reflecting the smaller back-bonding contribution of Ir(III) vs Fe(II) toward the NOSR ligand. This pioneering structural work was complemented by a comprehensive structural and spectroscopic study with a family of stable and water-soluble Ir^{III}–NOSR complexes, including DFT calculations and an estimation of comparative reactivity related to the N–S bond rupture *(73)*.

An alternative method for preparing bound-NOSR complexes consists of using the thiolates as nucleophiles toward the N-atom in bound nitrosyl complexes, such as nitroprusside. Addition reactions of diverse species such as OH^-, NH_3, N_3^-, N_2H_4, NH_2OH, and SO_3^{2-}, on the formally considered NO^+-ligand in nitroprusside have been widely studied mechanistically *(10)*, and this is also the case for the reactions with HS^- and several aliphatic thiolates, including those derived from mercaptosuccinic acid, cysteine, and glutathione, reaction (21):

$$\left[Fe(CN)_5(NO)\right]^{2-} + RS^- \rightleftharpoons \left[Fe(CN)_5(NOSR)\right]^{3-} \quad K_{21},\ k_{21},\ k_{-21} \tag{21}$$

The fast kinetics for the formation/dissociation of adducts formed with different RSH thiols have been measured using temperature-jump/stopped-flow methods by Johnson and Wilkins *(74)*. The second-order formation rate constants were found to be pH dependent, showing that only the RS^- species are reactive. The value of k_{21} varies little with the thiol type (3×10^3–4×10^4 M^{-1} s^{-1}) at 25°C, with similar $\triangle H^{\neq}$ values, ~33 kJ mol^{-1}. There is a much larger variation in the adduct dissociation rate constants k_{-21}

(from 12 to 3×10^3 s^{-1}). The establishment of the equilibrium reaction (21) is characterized by a marked color increase, followed by its fading in a slower time scale described initially by reaction (20) and subsequent decompositions. It should be remarked that the equilibrium constants K_{21} have only moderate values, and incomplete conversions of nitroprusside into the $[Fe(CN)_5(NOSR)]^{3-}$ complexes are usually achieved. Reaction (21) is markedly accelerated in the presence of excess thiolate, leading to $[Fe(CN)_5(NO^{\cdot})]^{3-}$ and disulfides, RSSR *(67)*. The reaction in Eq. (21) is also influenced by the presence of oxygen *(67,75)*.

6.2 Thionitrous Acid/Thionitrite

A biorelevant case of HSNO generation and reactivity has been reported by studying the reaction of NO_2^- with H_2S at pH 7.4, catalyzed by a Fe^{II}–porphyrin model complex. The Fe–NOSH intermediate could be characterized through cryospray, time-of-flight (TOF) ESI-MS detection. HSNO was proposed to be released from the iron center enabling the nitrosation of added bovine serum albumin. It was also presumed as the source of HNO generation. No evidence of S_2NO^- has been shown in this study *(76)*. Strong evidence for the coordination of HSNO and NOS^- by the $[Fe^{II}(CN)_5]^{3-}$ moiety is presented in Section 6.4.

6.3 Perthionitrite

Direct reaction between freshly generated aqueous S_2NO^- and hemoglobin (Hb) centers, also extended to myoglobin (Mb), has been very recently established *(58)*. By using deoxyHb^{II} and/or deoxygenated methemoglobin, Hb^{III}, the addition of free S_2NO^- rapidly produced nitrosyl hemoglobin, $Hb^{II}NO$, with additional formation of polysulfides HS_x^-, or HS_2^-, respectively. The studies were carried out using time resolved EPR and UV–vis methods, and also showed that heme-species without a vacant site, like $Hb^{II}CO$ or $Hb^{II}O_2$, did not produce bound NO, suggesting the necessary previous coordination of S_2NO^- to the metal center. The latter event has not been demonstrated however, and further mechanistic studies are in order. It is worth pointing out that the authors used the GSNO/H_2S reaction to generate free S_2NO^- with a subsequent degassing, thus assuring the elimination of the previously produced NO, formed through the reactivity of HSNO (see Section 5.4). On the other hand, remarkable evidence can be anticipated on the coordination of S_2NO^- to $[Fe^{II}(CN)_5]^{3-}$, as shown in Section 6.4.

6.4 The Gmelin Reaction, $[Fe(CN)_5(NO)]^{2-} + HS^-$

This 170-year-old reaction *(77)* is quite relevant for comparing the reactivity of HS^- vs RS^- as nucleophiles toward a common electrophile, complementing the analysis previously carried out for the transnitrosation reactions *(49)*. The Gmelin reaction is a complex process comprising the generation of an intense red–purple color upon mixing the reactants (λ_{max}, 535 nm, pH 12–13); the color develops in a less than or in a few seconds (depending on $[HS^-]$), followed by color fading in a slower time scale *(30)*. In this respect, the chemistry appears similar to that discussed in Section 6.1. The stoichiometric and mechanistic Gmelin features are strongly dependent on the pH and on O_2 availability *(34)*. S_8 is the exclusive final product of hydrosulfide oxidation *(78)*, not RSSR as found for RSNOs *(67,75)*. NH_3 and N_2O are the reduction products of bound nitrosyl: NH_3 is produced at all pH values but N_2O only at pH > 12. The hexacyanoferrate(II) anion, aqueous Fe(II,III), and/or Prussian-blue-type precipitates appear as the main final sinks for iron and cyanides *(30)*. The overall process comprises the build-up and decay of multiple intermediates, with particular controversial issues arising in the identification of the freshly formed I_{535} (the "red" species) and its prompt successor, I_{575}, the "blue" species formed in seconds in a pH-dependent way. Alternative views on their characterization and reactivity have been raised in the last 5 years by us *(30)* and others *(31–33)*. We are currently revisiting this reaction *(34)*, and we advance some new results here. We will summarize and present the information from the available interpretations, while aiming to present a balanced view.

In our previous work in 2011 *(30)*, we showed that the absorbance maxima and intensities evolving just after mixing the reactants depended on the molar ratio $R = [HS^-]/[Fe]$ and the pH. The values of λ_{max} for the emerging absorptions varied in the range of 535–570 nm in the pH range 8.5–12.5, in anaerobic conditions. Fig. 6 shows some typical absorbance-time profiles for $R = 30$.

The traces exhibited a characteristic biexponential form, with a fast increase of absorbance and a slower decrease. Lower conversions of nitroprusside into the colored adduct were achieved at the lower pH values. At constant pH, the following rate law has been established in the pH range studied by means of the initial rate method (i.e., by using the rising part of the curves): $v = d[A_d]/dt = k_{ad}\,[HS^-][NP]$, with A_d representing the colored adduct/s. The following equilibrium reactions (22–24), include the initial

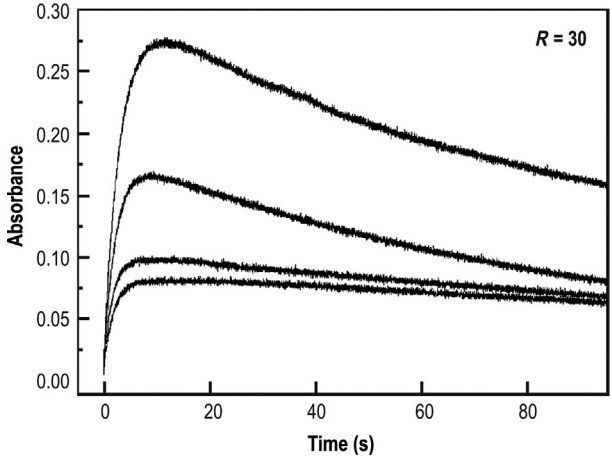

Fig. 6 Absorbance at 535 nm against time for the reaction of 0.05 mM $[Fe(CN)_5(NO)]^{2-}$ and HS^-, $R=30$. pH increases upward: 8.7, 9.5, 10.5, and 12.3. *Adapted from Quiroga, S. L.; Almaraz, A. E.; Amorebieta, V. T.; Perissinotti, L. L.; Olabe, J. A.* Chem. Eur. J. ***2011***, 17, *4145–4156. with permission of Wiley.*

addition step and the fast isomerization and deprotonation equilibria of the isomers:

$$\left[Fe(CN)_5(NO)\right]^{2-} + HS^- \rightleftharpoons \left[Fe(CN)_5(NOSH)\right]^{3-} \quad (22)$$

$$\left[Fe(CN)_5(NOSH)\right]^{3-} \rightleftharpoons \left[Fe(CN)_5(NSOH)\right]^{3-} \quad (23)$$

$$\left[Fe(CN)_5(NOSH)\right]^{3-} / \left[Fe(CN)_5(NSOH)\right]^{3-} \rightleftharpoons \left[Fe(CN)_5(NOS)\right]^{4-} + H^+ \quad (24)$$

By considering a mass-balance equation for the iron-containing species, we obtained the following parameters by fitting procedures: $k_{22}=190\ M^{-1}\ s^{-1}$ and $k_{-22}=0.30\ s^{-1}$ *(30)*. Finding that the addition of HS^- was a reversible process, in a similar way as occurs for thiolates *(74)*, had not been reported previously. Not unexpectedly, k_{22} was significantly smaller than k_{21}, given the lower nucleophilicity and polarizability of HS^- compared with RS^-. Remarkably, an unidentified intermediate with a value of pK_a of ~10.5 could be discerned from the kinetic analysis *(30)*. We have elaborated in Section 3 on the intermediacy of NOSH/NSOH/HNSO isomers interreacting with such a possible value of pK_a. The same would be the case here, with a mixture of rapidly reacting bound-NOSH species as described in reactions (23) and (24).

Our analysis implied the consideration that the rising absorbance traces *only* comprised the build-up of $[Fe(CN)_5(NOSH)]^{3-}$ and $[Fe(CN)_5(NOS)]^{4-}$. The $[Fe(CN)_5(NOSH)]^{3-}$ ion, predicted to be unstable by our DFT computations *(30)*, was tentatively (and incorrectly) assigned to the "blue" 570 nm species. At that time, we were unable to identify the bound $[S_2NO]^-$ ion, eventually being formed a few seconds after mixing. In 2012, Filipovic and Ivanovic-Burmazovic questioned our assignments on I_{535} ($[Fe(CN)_5(NOS)]^{4-}$) and I_{575} ($[Fe(CN)_5(NOSH)]^{3-}$) by working at pH 7.4 ($R = 34$) under anaerobic conditions *(31)*. They reported an *initial* absorption band at 535 nm (accompanied by a weaker one at 330 nm), also extensive to *all pHs*. $I_{535,330}$ subsequently decayed in a few seconds to a more stable intermediate, I_{570}. The slowness of the $I_{535} \rightarrow I_{570}$ change precluded assigning it to an acid–base transformation. The authors assigned I_{535} to $[Fe(CN)_5(NOSH)]^{3-}$, though I_{570} remained unidentified *(31)*. In 2013 the same authors elaborated a detailed mechanism *(32)* by working in *oxygenated* conditions at pH 7.4 and $R = 125$. I_{570} was traced to $[Fe^{II}(CN)_4(NCS)(H_2O)]^{3-}$, an ill-characterized intermediate, formed after the release of HNO from the iron center. New colored intermediates appeared that had not been observed under anaerobic conditions. A detailed evaluation of that proposal *(32)* is not offered herein, but may follow in time *(34)*.

We show in Fig. 7A our results at pH 8.9, with an absorbance-rise comprising the transformation $I_{535} \rightarrow I_{575}$; Fig. 7B shows the subsequent decay at 575 nm. A similar picture evolves in Fig. 8A and B, with formation of I_{575} in the decay region (a greater value was achieved earlier by I_{535} owing to the

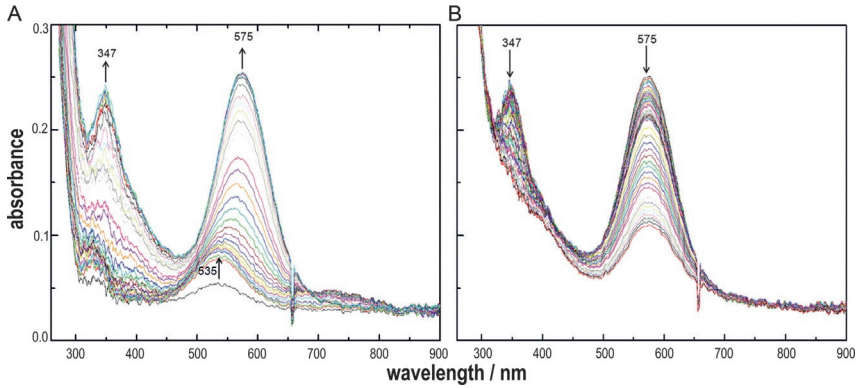

Fig. 7 (A) Successive UV–vis spectra after mixing 0.1 mM $[Fe(CN)_5(NO)]^{2-}$ and HS^-, pH 8.9, $R = 30$. (B) Successive UV–vis spectra, same conditions as in (A), ~20 s after mixing.

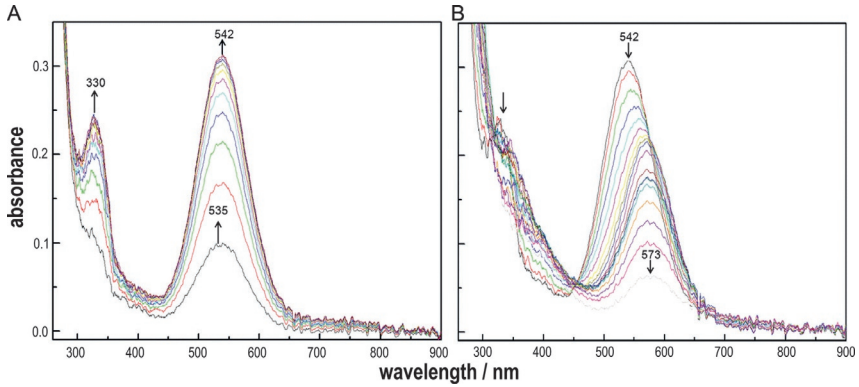

Fig. 8 (A) Successive UV–vis spectra after mixing 0.1 mM $[Fe(CN)_5(NO)]^{2-}$ and HS^-, pH 8.9, $R = 100$. (B) Successive UV–vis spectra, same conditions as in (A), ~1.5 s after mixing.

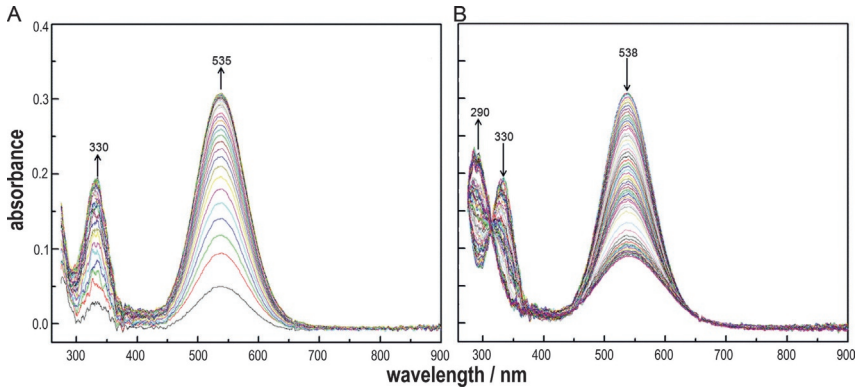

Fig. 9 (A) Successive UV–vis spectra after mixing 0.05 mM $[Fe(CN)_5(NO)]^{2-}$ and HS^-, pH 12, $R = 100$. (B) Successive UV–vis spectra, same conditions as in (A), ~6 s after mixing.

faster second-order build-up of $[Fe(CN)_5(NOSH)]^{3-}$). We briefly highlight the onset of an early absorption at 347 nm, assigned to $[Fe(CN)_5(NO^{\cdot})]^{3-}$ *(69)*. In sharp contrast, Fig. 9 at pH 12 shows the formation of *only* I_{535}, without any feature at 575 nm. Under these conditions, I_{535} was moderately stable ($t_{½} \sim 60$ s) and we assigned it to $[Fe(CN)_5(NOS)]^{4-}$, quantitatively generated according to reactions (18–20), under irreversible conditions for reaction (20). These observations allowed an estimate of $\varepsilon = 6000\ M^{-1}\ cm^{-1}$ for the thionitrite-bound complex, in agreement with results of DFT calculations *(30)*. The absorption features of $[Fe(CN)_5(NOS)]^{4-}$ are consistent with those for the $[Fe(CN)_5(NOSR)]^{3-}$ complexes *(68, 74)*.

Another development in the mechanistic discussion was provided by Wu and coworkers in 2015 *(33)*. They used 1.2 mM $[Fe(CN)_5(NO)]^{2-}$, a slight excess of HS^- ($R = 3$), and aerobic conditions. At pH 12, the initially formed band with λ_{max} at 542 nm was traced to $[Fe(CN)_5(NOS)]^{4-}$, also described by a ^{17}O NMR peak at 1028 ppm. The color faded along with a shift of λ_{max} up to ~555 nm, fully attained 6 min after mixing. Later on, the fading progressed at 555 nm for more than 1 h (cf. fig. 1c in Ref. *(33)*). The authors fitted the results (fig. 1d) as a two-step process with values of $t_{½} = 1.5$ min (decay at 542 nm with assumed build-up at 570 nm), and $t_{½} = 90$ min (decay at 570 nm), suggesting that a 542 nm → 570 nm conversion was onset during the first rapid step. However, as clarified earlier, fig. 1c shows the intermediate maximum at 555 nm, not at 570 nm. Certainly, the fitting plot does not show that the 570 nm maximum is ever attained at all for the underlying conditions *(33)*.

The initial UV–vis 542 nm → 555 nm change correlated with the decay of the ^{17}O peak at 1028 ppm and its replacement by a new signal emerging at 938 ppm, fully attained in 3 min. The authors proposed that the new species rapidly formed upon $[Fe(CN)_5(NOS)]^{4-}$ decay was $[Fe(CN)_5(NOS_2)]^{4-}$, and added new experimental evidence: (1) By working at pH 7.4 (other conditions as described earlier) the red–violet color (λ_{max}, 542 nm) could not be captured; instead the solution became "immediately" blue, with λ_{max} at 577 nm. (2) A further experiment in which 25 mM $[Fe(CN)_5(NO)]^{2-}$ was mixed with HS_2^- at pH 11 ($R = 3$) led also "immediately" to the blue species. The color decayed subsequently in the minute time scale.

Given the latter results on the significant pH influence, as well as our very recent report on the identification of S_2NO^- as a consequence of the high reactivity of HS_2^- *(49)*, we looked at the Gmelin analog reaction by using HS_2^- instead of HS^-. In our hands, transparent yellow solutions resulting from the direct reaction of $[Fe(CN)_5(NO)]^{2-}$ with aqueous Na_2S_2 could only be obtained in the pH range 9–12; colloidal sulfur was always rapidly produced by mixing at pH values <9 *(34)*. Fig. 10 displays a set of successive spectra, obtained at pH 12, with two well-defined regions: an initial fast absorbance increase at 550 nm ($t_{½}$, 2 s), is followed by a slower transformation ($t_{½}$, 20 s) generating a band maximum centered at 575 nm. The same pattern was observed in all of the pH range utilized. The inset shows a comparison of the spectral features of the final product (λ_{max}, 575 nm) with the one produced in the Gmelin reaction at pH 7, a remarkable coincidence.

A UV–vis spectrum of $[Fe(CN)_5(NOS_2)]^{4-}$ was obtained by using the *real-time* TD-DFT/QM-MM methodology described earlier *(49)*. Fig. 11

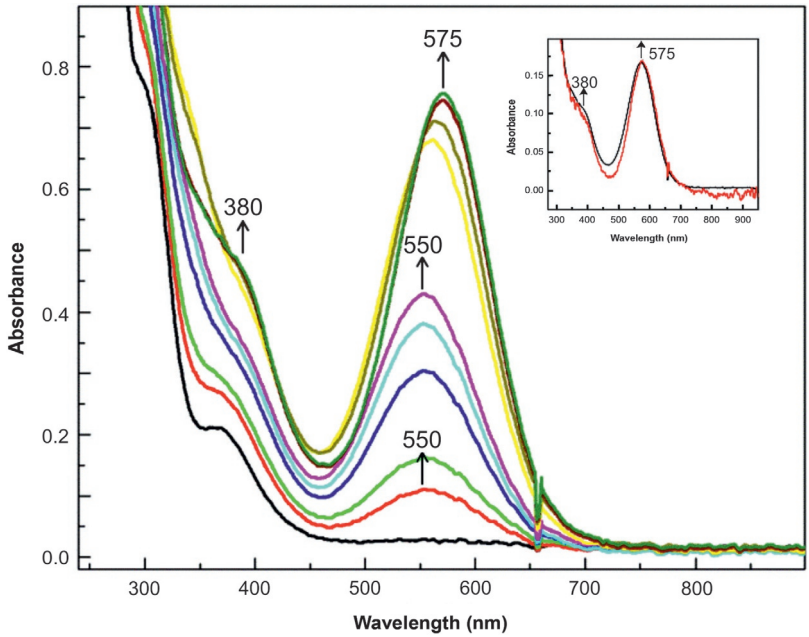

Fig. 10 Successive spectra for the reaction of 0.05 mM $[Fe(CN)_5(NO)]^{2-}$ with aqueous Na_2S_2, pH 12, $R \sim 1$ *(34)*. The first spectrum in black was measured 0.5 s after mixing and corresponds to buffered HS_2^-. The next five spectra (*red* to *violet*) correspond to reaction times: 1.4, 2.7, 4.0, 5.3, and 6.5 s.

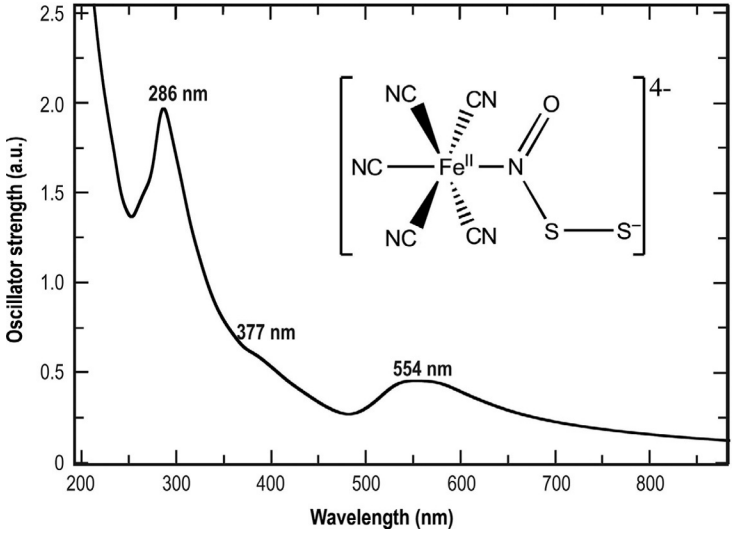

Fig. 11 Real-time TD-DFT/QM-MM calculated spectrum for $[Fe(CN)_5(NOS_2)]^{4-}$ in water, performed at the same level of theory as described in Ref. *(49)*.

shows a spectrum that converged after several months yielding a broad band centered at ~552 nm. Overall, a preliminary consideration of our results and those of Wu and coworkers *(33)* suggests that the perthionitrite complex $[Fe(CN)_5(NOS_2)]^{4-}$ absorbs at ~550 nm, and that I_{550} could transform in a slower way into a polysulfide-bound species $[Fe(CN)_5(NOS_x)]^{4-}$, I_{575}. The conversion would require the availability of sulfane sulfur (S^o) in the medium, a feasible situation in the pH range 7–9 due to the decomposition of HS_2^- and ensuing formation of polysulfides, as discussed in Section 4.

A summary of the overall mechanistic features involves identifying $[Fe(CN)_5(NOSH)]^{3-}$ and $[Fe(CN)_5(NOS)]^{4-}$ as the initial intermediates formed in a pH-dependent way. Both anions have similar band maxima at ~535–540 nm, a similar situation reported earlier for free HSNO and NOS^-. The novel picture deals with the pH-dependent reactivity of both species toward the N–S bond homolysis. On the one hand, $[Fe(CN)_5(NOS)]^{4-}$ is moderately stable at pH values ≥ 11, affording a decay of the 535-nm absorption with a $t_{½}$ ~60 s, yielding $[Fe(CN)_5(NO^{\cdot})]^{3-}$ (detected by UV–vis and EPR), probably $[Fe(CN)_5(HNO)]^{3-}$, and $HS^{\cdot}$ radicals that are a source of HS_2^-, as well as NH_3 and N_2O *(30)*. The decay at 535 nm shows a subsequent very slow step comprising the decomposition of the $[Fe(CN)_5(NO)]^{3-}$ intermediate ($k \sim 10^{-5}\ s^{-1}$), also producing additional N_2O *(30)*. On the other hand, and in sharp contrast, working in the pH range 7–10 allows I_{575} emerging in a few seconds after mixing, associated with the reactivity of $[Fe(CN)_5(NOSH)]^{3-}$ ($t_{½} \sim 6$ s). In addition to reactions (22–24), we define reaction (25) by considering similar arguments as exposed above for the generation of free S_2NO^-.

$$\left[Fe(CN)_5(NOSH)\right]^{3-} / \left[Fe(CN)_5(NSOH)\right]^{3-} + HS_2^- \rightleftharpoons \left[Fe(CN)_5(NOS_2)\right]^{4-} + HS^- + H^+ \quad (25)$$

Although the main question related to the identification of the "red" and "blue" intermediates seems to be correctly focused by highlighting the different chemistries of HS^- and HS_2^- as nucleophilic reagents, solving the ambiguities on the clear identification of I_{550} and I_{570} must be pursued. A relevant question deals with I_{550} being either a true intermediate species or an artifact appearing because of band-overlap during the 535 nm → 575 nm transformation. Our current work *(34)* is focused on a deeper mechanistic probe, also searching for the influence of O_2 on the early onset of new colored intermediates, the chemistry of HNO generation and N_2O-release, as well as on the role of the 1-electron reduced

$[Fe(CN)_5(NO)]^{3-}/[Fe(CN)_4(NO)]^{2-}$ radical-complexes in the route to final products.

7. CONCLUSIONS

The thionitrous acid HSNO intermediate (in fact, a mixture of thermally accessible tautomers in the aqueous solutions) has been reasonably well identified by MS and UV–vis spectroscopies, aided by theoretical calculations. HSNO survives sufficiently after its generation as an initial product of the transnitrosation reaction of GSNO with H_2S. HSNO affords a rich chemistry toward different substrates, either leading to NO, probably HNO or eventually other transnitrosation products. It can also generate S_2NO^- through the reaction with early generated HS_2^- in the medium. Although the biologically significant signaling ability of S_2NO^- has not been demonstrated yet *(25,45)*, the identity and survival of S_2NO^- in water for minutes/hours are well established facts *(49,58)*. However, the latter assertion is still strongly questioned in the very recent reports by Filipovic and Ivanovic-Burmazovic *(60,79,80)*. Indeed, a better knowledge of the O_2-dependent decay routes of S_2NO^- is needed in the time scale of minutes/hours, giving either NO, HNO/N_2O or other hybrid species, and N-reduced products. The recently reported reactivity of S_2NO^- in aprotic solvents toward CN^-, GSH, and H_2S *(60)* ought to be contrasted with measurements in aqueous media in search for a pH dependence. The coordinated "Gmelin" species $[Fe^{II}(CN)_5(NOSH)]^{3-}$ and $[Fe^{II}(CN)_5(NOS)]^{4-}$ appear to be well-characterized reactive anions ("red" intermediates absorbing at 535–540 nm), though the true absorption maximum of the "blue" intermediate $[Fe^{II}(CN)_5(NOS_2)]^{4-}$ formed in the pH range 7–10 is still uncertain. Unraveling the chemistry of the latter species and of other intermediates is still a main challenge for a thorough, complete description of the Gmelin process.

ACKNOWLEDGMENTS

We thank the University of Buenos Aires and CONICET for financial support. We are grateful to Dr. Valentín T. Amorebieta for his experimental contribution on the Gmelin reaction, and to Dr. Sara E. Bari for fruitful discussions.

REFERENCES

1. Wang, R. *Physiol. Rev.* **2012**, *92*, 791–896.
2. Fukuto, J. M.; Carrington, S. J.; Tantillo, D. J.; Harrison, J. G.; Ignarro, L. J.; Freeman, B. A.; Chen, A.; Wink, D. A. *Chem. Res. Toxicol.* **2012**, *25*, 769–793.

3. Ignarro, J. L. *Nitric Oxide: Biology and Pathobiology*. Academic Press: San Diego, 2000.
4. Calderwood, A.; Kopriva, S. *Nitric Oxide* **2014**, *41*, 72–78.
5. Bari, S. E.; Olabe, J. A. In *Gasotransmitters in Plants. The Rise of a New Paradigm in Cell Signalling*; Lamattina, L., García-Mata, C., Eds.; Springer International Publishing: Switzerland, 2016; pp 289–327. ch. 14.
6. Bari, S. E.; Olabe, J. A.; Slep, L. D. *Adv. Inorg. Chem.* **2014**, *67*, 87–144.
7. Lehnert, N.; Berto, T. C.; Galinato, M. G. I.; Goodrich, L. E. In *The Handbook of Porphyrin Science*; Kadish, K. M., Smith, K. M., Guilard, R., Eds.; Vol. 14 ;World Scientific: New Jersey, 2011; pp 1–247. 63.
8. Li, Q.; Lancaster, J. R., Jr. *Nitric Oxide* **2013**, *35*, 21–34.
9. Mishanina, T. V.; Libiad, M.; Banerjee, R. *Free Rad. Biol. Med.* **2015**, *11*, 457–464.
10. Olabe, J. A. *Adv. Inorg. Chem.* **2004**, *55*, 61–126.
11. Toohey, J. L. *Anal. Biochem.* **2011**, *413*, 1–7.
12. Ono, K.; Akaike, T.; Sawa, T.; Kumagai, Y.; Wink, D. A.; Tantillo, D. J.; Hobbs, A. J.; Nagy, P.; Xian, M.; Lin, J.; Fukuto, J. M. *Free Rad. Biol. Med.* **2014**, 77, 82–94.
13. Cuevasanta, E.; Moller, M. N.; Alvarez, B. *Arch. Biochem. Biophys.* **2017**, *617*, 9–25.
14. Whiteman, M.; Li, L.; Kostetski, I.; Chu, S. H.; Siau, J. L.; Bhatia, M.; Moore, P. K. *Biochem. Biophys. Res. Commun.* **2006**, *343*, 303–310.
15. Yong, Q. C.; Cheong, J. L.; Hua, F.; Deng, L. W.; Khoo, Y. M.; Lee, H. S.; Perry, A.; Wood, M.; Whiteman, M.; Bian, J. S. *Antioxid. Redox Signal* **2011**, *14*, 2081–2091.
16. Coletta, C.; Papapetropoulos, A.; Erdelyi, K.; Olah, G.; Modis, K.; Panopoulos, P.; Asimakopoulou, A.; Gero, D.; Sharina, I.; Martin, E.; Szabo, C. *Proc. Natl. Acad. Sci. U.S.A* **2012**, *109*(23), 9161–9166.
17. Fago, A.; Jensen, F. B.; Tota, B.; Feelisch, M.; Olson, K. R.; Helbo, S.; Lefevre, S.; Mancardi, D.; Palumbo, A.; Sandvik, G. K.; Skovgaard, N. *Comp. Biochem. Physiol. A* **2012**, *162*, 1–6.
18. Lo Faro, M. L.; Fox, B.; Whatmore, J. L.; Winyard, P. G.; Whiteman, M. *Nitric Oxide* **2014**, *41*, 38–47.
19. Berenyiova, A.; Grman, M.; Mijuskovic, A.; Stasko, A.; Misak, A.; Nagy, P.; Ondriasova, E.; Cacanyiova, S.; Brezova, V.; Feelisch, M.; Ondrias, K. *Nitric Oxide* **2015**, *46*, 123–130.
20. Grman, M.; Jawad Nassim, M.; Leontiev, R.; Misak, A.; Jakusova, V.; Ondrias, K.; Jacob, C. *Antioxidants* **2017**, *6*, 14.
21. King, S. B. *Free Rad. Biol. Med.* **2013**, *55*, 1–7.
22. Nonella, M.; Huber, J. R.; Ha, T. K. *J. Phys. Chem.* **1987**, *91*, 5203–5209.
23. Seel, F.; Kuhn, R.; Simon, G.; Wagner, M.; Krebs, B.; Dartmann, M. *Z. Naturforsch.* **1985**, *40b*, 1607–1617.
24. Filipovic, M. R.; Miljkovic, J. L.; Nauser, T.; Royzen, M.; Klos, K.; Shubina, T.; Koppenol, W. H.; Lippard, S. J.; Ivanović-Burmazović, I. *J. Am. Chem. Soc.* **2012**, *134*, 12016–12027.
25. Wedmann, R.; Zahl, A.; Shubina, T. E.; Durr, M.; Heinemann, F. W.; Eberhard, B.; Bugenhagen, C.; Burger, P.; Ivanović-Burmazović, I.; Filipovic, M. R. *Inorg. Chem.* **2015**, *54*, 9367–9380.
26. Cortese-Krott, M. M.; Fernandez, B. O.; Santos, J. L. T.; Mergia, E.; Grman, M.; Nagy, P.; Kelm, M.; Butler, A.; Feelisch, M. *Redox Biol.* **2014**, *2*, 234–244.
27. Cortese-Krott, M. M.; Kuhnle, G. G.; Dyson, A.; Fernandez, B. O.; Grman, M.; DuMond, J. F.; Barrow, M. P.; McLeod, G.; Nakagawa, H.; Ondrias, K.; Nagy, P.; King, S. B.; Saavedra, J. E.; Keefer, L. K.; Singer, M.; Kelm, M.; Butler, A. R.; Feelisch, M. *Proc. Natl. Acad. Sci. U.S.A.* **2015**, *112*, 4651–4660.
28. Broniowska, K. A.; Hogg, A. *Antioxid. Redox Signal.* **2012**, *17*, 969–980.
29. Szacilowski, K.; Stasicka, Z. *Progr. React. Kin. Mech.* **2001**, *26*, 1–58.

30. Quiroga, S. L.; Almaraz, A. E.; Amorebieta, V. T.; Perissinotti, L. L.; Olabe, J. A. *Chem. Eur. J.* **2011**, *17*, 4145–4156.
31. Filipovic, M. R.; Ivanovic-Burmazovic, I. *Chem. Eur. J.* **2012**, *18*, 13538–13540.
32. Filipovic, M. R.; Eberhardt, M.; Prokopovic, V.; Mijuskovic, A.; Orescanin Dusic, O.; Reeh, P. H.; Ivanovic-Burmazovic, I. *J. Med. Chem.* **2013**, *56*, 1499–1508.
33. Gao, Y.; Toubaei, A.; Kong, X.; Wu, G. *Chem. Eur. J.* **2015**, *21*, 17172–17177.
34. Olabe, J.A., 3rd European Colloquium on Inorganic Reaction Mechanisms, ECIRM 2016, June 21−25, Kraków. Oral presentation, *unpublished work*.
35. Arulsamy, N.; Bohle, D. S.; Butt, J. A.; Irvine, G. J.; Jordan, P. A.; Sagan, E. *J. Am. Chem. Soc.* **1999**, *121*, 7115–7123.
36. Hu, Y.; Stanbury, D. M. *Inorg. Chem.* **2016**, *55*, 7797–7803.
37. Das, T. N.; Huie, R. E.; Neta, P.; Padmaja, S. *J. Phys. Chem. A* **1999**, *103*, 5221–5226.
38. Koppenol, W. H. *Inorg. Chem.* **2012**, *51*, 5637–5641.
39. Arnelle, D. R.; Stamler, J. S. *Arch. Biochem. Biophys.* **1999**, *318*(2), 279–285.
40. Singh, S. P.; Wishnok, J. S.; Keshive, M.; Deen, W. M.; Tannenbaum, S. R. *Proc. Natl. Acad. Sci. U.S.A.* **1996**, *93*, 14428–14433.
41. Wong, P. S. Y.; Hyun, J.; Fukuto, J. M.; Shirota, F. N.; DeMaster, E. G.; Shoeman, D. W.; Nagasawa, H. T. *Biochemistry* **1998**, *37*, 5362–5371.
42. Cortese-Krott, M. M.; Butler, A.; Woollins, J. D.; Feelisch, M. *Dalton Trans.* **2016**, *45*, 5908–5919.
43. Ivanova, L. V.; Anton, B. J.; Timerghazin, Q. K. *Phys. Chem. Chem. Phys.* **2014**, *16*, 8476–8486.
44. Nava, M.; Martin-Drummel, M. A.; Lopez, C. A.; Crabtree, K. N.; Womack, C. C.; Nguyen, T. L.; Thorwirth, S.; Cummins, C. C.; Stanton, J. F.; McCarthy, M. C. *J. Am. Chem. Soc.* **2016**, *138*, 11441–11444.
45. Koppenol, W. H.; Bounds, P. L. *Arch. Biochem. Biophys.* **2017**, *617*, 3–8.
46. Seel, F.; Wagner, M. *Z. Anorg. Allg. Chem.* **1988**, *558*, 189–192.
47. Bohle, D. S.; Hansert, B.; Paulson, S. C.; Smith, B. D. *J. Am. Chem. Soc.* **1994**, *116*, 7423–7424.
48. Szacilowski, K.; Chmura, A.; Stasicka, Z. *Coord. Chem. Rev.* **2005**, *249*, 2408–2436.
49. Marcolongo, J. P.; Morzan, U. N.; Zeida, A.; Scherlis, D. A.; Olabe, J. A. *Phys. Chem. Chem. Phys.* **2016**, *18*, 30047–30052.
50. Slep, L. D.; Pollak, S.; Olabe, J. A. *Inorg. Chem.* **1999**, *38*, 4369–4371.
51. Munro, A. P.; Williams, D. L. H. *J. Chem. Soc. Perkin* **2000**, *21*, 1794–1797.
52. Armstrong, D. A.; Huie, R. E.; Koppenol, W. H.; Lymar, S. V.; Merényi, G.; Neta, P.; Ruscic, B.; Stanbury, D. M.; Steenken, S.; Wardman, P. *Pure Appl. Chem.* **2015**, *87*, 1139–1150.
53. Eberhard, M.; Dux, M.; Namer, B.; Miljkovic, J.; Cordasic, N.; Will, C.; Kichko, T. L.; de la Roche, J.; Fischer, M.; Suarez, S. A.; Bikiel, D.; Dorsch, K.; Leffler, A.; Babes, A.; Lampert, A.; Lennerz, J. K.; Jacobbi, J.; Marti, M. A.; Doctorovich, F.; Hoggestat, E. D.; Zygmunt, P. M.; Ivanovic-Burmazovic, I.; Messlinger, K.; Reeh, P.; Filipovic, M. R. *Nat. Commun.* **2014**, *5*, 4381.
54. Nagy, P. *Methods Enzymol.* **2015**, *554*, 3–29.
55. Cuevasanta, E.; Zeida, A.; Carballal, S.; Wedmann, R.; Morzan, U. N.; Trujillo, M.; Radi, R.; Estrin, D. A.; Filipovic, M. R.; Alvarez, B. *Free Radic. Biol. Med.* **2015**, *80*, 93–100.
56. Giggenbach, W. *Inorg. Chem.* **1971**, *11*, 1333–1338.
57. Bailey, T. S.; Henthorn, H. A.; Pluth, M. D. *Inorg. Chem.* **2016**, *55*, 12618–12625.
58. Bolden, C.; King, S. B.; Kim-Shapiro, D. B. *Free Rad. Biol. Med.* **2016**, *99*, 418–425.
59. Estrín, D. A.; Baraldo, L. M.; Slep, L. D.; Barja, B. C.; Olabe, J. A. *Inorg. Chem.* **1996**, *35*, 3897–3903.

60. Wedmann, R.; Ivanovic-Burmazovic, I.; Filipovic, M. R. *Interface Focus* **2017**, *7*, 20160139.
61. Cuevasanta, E.; Lange, M.; Bonanata, J.; Coitiño, E. L.; Ferrer-Sueta, G.; Filipovic, M. R.; Alvarez, B. *J. Biol. Chem.* **2015**, *290*, 26866–26880.
62. Everett, S. A.; Schoneich, C.; Stewart, J. H.; Asmus, K. D. *J. Phys. Chem.* **1992**, *96*, 306–314.
63. Shafirovich, V.; Lymar, S. V. *Proc. Natl. Acad. Sci. U.S.A.* **2002**, *99*, 7340–7345.
64. Smulik, R.; Debski, D.; Zielonka, J.; Michalowski, B.; Adamus, J.; Marcinek, A.; Kalyanaraman, B.; Sikora, A. *J. Biol. Chem.* **2014**, *289*, 35570–35581.
65. Pokkrebyshev, G. A.; Shafirovich, V.; Lymar, S. V. *J. Am. Chem. Soc.* **2008**, *112*, 8295–8302.
66. Frost, A. A.; Pearson, R. G. *Kinetics and Mechanism: A Study of Homogeneous Chemical Reactions*, 2nd ed.; John Wiley & Sons: New York, London, 1961.
67. Szacilowski, K.; Wanat, A.; Barbieri, A.; Wasiliewska, E.; Witko, M.; Stochel, G.; Stasicka, Z. *New J. Chem.* **2002**, *26*, 1495–1502.
68. Szacilowski, K.; Stochel, G.; Stasicka, Z.; Kisch, H. *New J. Chem.* **1997**, *21*, 893–902.
69. Schwane, J. D.; Ashby, M. T. *J. Am. Chem. Soc.* **2002**, *124*, 6822–6823.
70. Gao, Y.; Mossing, B.; Wu, G. *Dalton Trans.* **2015**, *44*, 20338–20343.
71. Andreasen, L. V.; Lorkovic, I. M.; Richter-Addo, G. B.; Ford, P. C. *Nitric Oxide* **2002**, *6*, 228–237.
72. Perissinotti, L. L.; Estrin, D. A.; Leitus, G.; Doctorovich, F. *J. Am. Chem. Soc.* **2006**, *128*, 2512–2513.
73. Perissinotti, L. L.; Leitus, G.; Shimon, L.; Estrin, D.; Doctorovich, F. *Inorg. Chem.* **2008**, *47*, 4723–4733.
74. Johnson, M. D.; Wilkins, R. G. *Inorg. Chem.* **1984**, *23*, 231–235.
75. Morando, P. J.; Borghi, E. B.; de Schteingart, L. M.; Blesa, M. A. *J. Chem. Soc. Dalton Trans.* **1981**, (2), 435–440.
76. Miljkovic, J.; Kenkel, I.; Ivanovic-Burmazovic, I.; Filipovic, M. *Angew. Chem. Int. Ed.* **2013**, *52*(46), 12061–12064.
77. Playfair, L. *Annalen* **1850**, *74*, 317.
78. Butler, A. R.; Calsy-Harrison, A. M.; Glidewell, C.; Sorensen, P. E. *Polyhedron* **1988**, *7*, 1197–1202.
79. Ivanovic-Burmazovic, I. In *The Chemistry and Biology of Nitroxyl (HNO)*; Doctorovich, F., Farmer, P. J., Marti, M. A., Eds.; Elsevier Inc., 2017; pp 67–104, Amsterdam, Netherlands. ISBN: 978-0-12-800934-5. ch. 5.
80. Filipovic, M. In *The Chemistry and Biology of Nitroxyl (HNO)*; Doctorovich, F., Farmer, P. J., Marti, M. A., Eds.; Elsevier Inc., 2017; pp 105–126, Amsterdam, Netherlands. ISBN: 978-0-12-800934-5. ch. 6.